Cite this: DOI: 10.1039/c0xx00000x

www.rsc.org/xxxxxx

PAPER

Electroactive carbon nanoforms: a comparative study via sequential arylation and click chemistry reactions†‡

Jaime Mateos-Gil,[§a] Laura Rodríguez-Pérez,[§a] María Moreno Oliva,[§b] Georgios Katsukis,[b] Carlos Romero-Nieto,[b,c] Mª Ángeles Herranz,*[a] Dirk M. Guldi*[b] and Nazario Martín*[a,d]

Received (in XXX, XXX) Xth XXXXXXXXX 20XX, Accepted Xth XXXXXXXXX 20XX
DOI: 10.1039/b000000x

The reactivity of several carbon nanoforms (CNF), single-walled carbon nanotubes (SWCNT), multi-walled carbon nanotubes (MWCNT) and graphene, has been investigated through a combination of arylation and click chemistry Cu^{I}-mediated azide-alkyne cycloaddition (CuAAC) reactions. The approach is based on the incorporation of electroactive π-extended tetrathiafulvalene (exTTF) units into the triazole linkers to modulate the electronic properties of the obtained conjugates. The introduction of strain, by bending the planar graphene sheet into a 3D carbon framework, is responsible of the singular reactivity observed in carbon nanotubes. The formed nanoconjugates were fully characterized by analytical, spectroscopic, and microscopic techniques (TGA, FTIR, Raman, UV-Vis-NIR, cyclic voltammetry, TEM and XPS). In the case of SWCNT conjugates, where the functionalization degree is higher, a series of steady-state and time resolved spectroscopy experiments revealed a photoinduced electron transfer from the exTTF unit to the electron-accepting SWCNT.

Introduction

With the advent of nanoscience and nanotechnology, carbon nanoforms, including fullerenes, carbon nanotubes, and graphene, have become the most popular nanomaterials due to their excellent mechanical, electronic, and thermal properties.[1] In particular, the successful isolation of single-layer graphene in 2004 caused a worldwide revolution aiming at the utilization of its unique structural and electronic properties in fields such as nanoelectronics, biosensors, supercapacitors, catalysis, nanomedicine, intercalation materials or polymer composites just to name a few.[2] Likewise, the appealing features of fullerenes[3] and carbon nanotubes (CNT)[4] also make them attractive building blocks for the aforementioned applications.

Two major drawbacks hamper, however, the application of CNT and graphene for practical purposes, namely their lack of solubility in common solvents and their relative inert surfaces. To overcome such setbacks, both covalent and non-covalent chemical modifications have been investigated in recent years.[5] On one hand, the non-covalent functionalization of CNT and graphene endows them with satisfactory solubility, while conserving their major structural characteristics. In most cases, the stability of the conjugates is, nevertheless, strongly influenced by the experimental conditions (solvents, pH, temperature, etc.).[6] The covalent functionalization, on the other hand, results in stable products, but implies the saturation of some of the sp^2 carbons of the CNFs' framework.[7] As a matter of fact, the electronic properties are accordingly impacted.

At the fundamental level, the chemical reactivity of sp^2-hybridized carbons is affected by the curvature, which alters the distribution of electron density in graphene and CNT. The chemical inertness of graphene can be easily understood on the basis of its planar framework, although its reactivity increases at the edges compared with the basal plane. For CNT, a direct correlation between tube diameter and reactivity exists. The pyramidalization angle among carbon bonds, that is, the difference between the sigma-pi orbital angle and 90º, and the π-orbital misalignment between carbon atoms decrease as the diameter increases, rendering small-diameter CNT more reactive than large-diameter CNT.[8]

Despite the fact that the covalent chemistry of carbon nanoforms has been intensively probed, to date, only a few studies focus on the comparative assays regarding these carbon frameworks.[9] Considering, for example, the basic details of chemical reactivity regarding either flat or curved sp^2-hybridized carbon materials different consequences should stem from their chemical functionalization.

The thrust of the present study is to perform a systematic and comparative analysis between the general reactivity of different types of CNT and graphene in light of benchmark reactions, which allows evaluating the properties of the different products. The reaction of all CNF with diazonium salts of aromatic compounds, bearing also alkyne functional groups, yields directly arylated derivatives that further react in a click process. Specifically, the combination of arylation and Cu-catalyzed Huisgen 1,3-dipolar cycloaddition of azides and alkynes (CuAAC) is widely applicable in organic and supramolecular chemistry and has recently been employed with great success in the area of CNT and graphene chemistry.[10] In addition, π-extended tetrathiafulvalenes (9,10-bis(1,3-dithiol-2-ylidene)-9,10-dihydro-

anthracene, exTTF) are powerful electron donors with have been successfully used for preparing new photoinduced electron transfer systems and solar energy conversion devices.[11] exTTF has been widely used to form electroactive architectures when linked to fullerenes and CNTs. Importantly, efficient electronic communication between the carbon nanoforms and exTTF has been documented for the ground and excited states by means of steady-state as well as time-resolved spectroscopies.[12,13]

Results and discussion

The synthesis of the different CNF-exTTF conjugates is described in Scheme 1. Note that the representation provides only a simplified view of the starting materials, namely SWCNT, MWCNT, and graphene. Following a previously reported procedure,[14] exTTFs were endowed with azido groups, which were subjected to a click chemistry reaction with the terminal ethynyl groups of the desired carbon nanostructures.

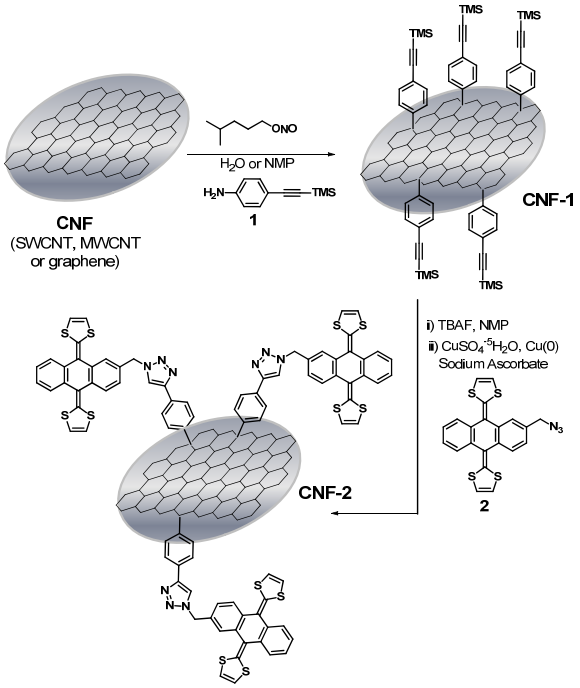

Scheme 1. Synthetic route towards functionalized CNF considering Tour conditions (CNF-1) and the click chemistry CuAAC protocol (CNF-2).

Regarding the introduction of ethynyl functionalities into the CNFs, the π-electronic systems of SWCNT, MWCNT and graphene were covalently modified via aryl diazonium chemistry.[15] This radical addition reaction affords intermediates that are decorated with phenylethynyl groups, when 4-[(trimethylsilyl)ethynyl]aniline is used as starting material. SWCNTs and MWCNTs were reacted following the well stablished procedure reported by Tour *et al.*[16] using water as reaction medium, in the presence of isoamyl nitrite and 4-[(trimethylsilyl)ethynyl]aniline, affording **SWCNT-1** and **MWCNT-1**. This functionalization method has been slightly modified when using graphene as the starting nanocarbon. To this end, the pristine graphene material was obtained through graphite exfoliation in *N*-methylpyrrolidone (NMP) following Coleman's procedure toward few-layered graphene suspensions with high degree of purity. To simplify the discussions we will keep referring from here on to graphene.[17] Such a graphene suspension in NMP was immediately reacted with 4-[(trimethylsilyl)ethynyl] aniline and isoamyl nitrite, which formed *in situ* the corresponding aryl diazonium salt, and, which yielded the covalent graphene conjugates. Notably, this process was followed by a second cycle of the same Tour reaction to increase the number of functional groups anchored onto the basal plane of graphene (**GR-1**).

Deprotection of the alkyne groups with tetrabutylammonium fluoride (TBAF) and subsequent Cu(I)-catalyzed 1,3-dipolar cycloaddition reaction with azido exTTF **2** was carried out *in situ* under thermal conditions for the three carbon nanoconjugates affording **SWCNT-2**, **MWCNT-2** and **GR-2**.

The protected alkyne groups anchored on the three intermediate carbon nanoforms skeletons were readily identified by Fourier transform infrared spectroscopy (FTIR). The stretching mode of the acetylenic spacer, ν(C≡C), appears as a weak band around 2200-2100 cm^{-1}, a region where very few organic compounds show IR-active modes.[18] The appearance of this band at 2159 cm^{-1} for **SWCNT-1** (Figure S1), at 2156 cm^{-1} for **MWCNT-1** (Figure 1), and at 2165 cm^{-1} for **GR-1** (Figure S2) corroborates the presence of alkynes on the corresponding surfaces. These bands disappear after CuAAC reaction with azido-exTTF **2** for all of the carbon nanostructures, that is, **SWCNT-2**, **MWCNT-2**, and **GR-2**. This is due to the formation of triazole rings. The characteristic bands of the skeletal in-plane vibration is seen at 1599 cm^{-1} for SWCNT, at 1580 cm^{-1} for MWCNT, and at 1583 cm^{-1} for graphene.[19] As a complement, the aliphatic C–H stretching mode located between 2850 and 2950 cm^{-1} and the C–H bending mode at around 1250–1500 cm^{-1} are discernable in all the intermediate and final nanoconjugates.

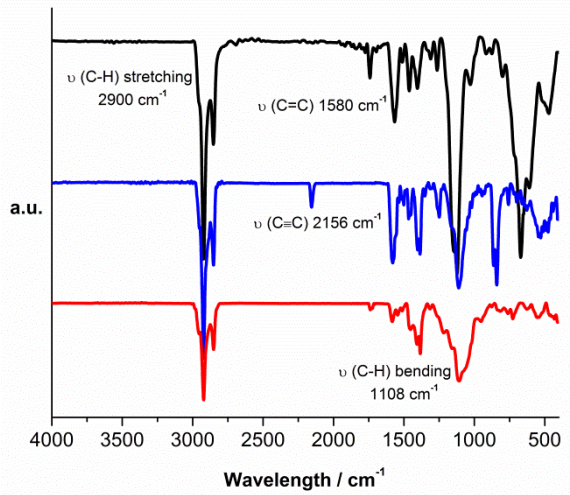

Figure 1. FTIR spectra of **MWCNT-2** (red), **MWCNT-1** (blue), and pristine MWCNT (black).

While FTIR spectroscopy reveals important chemical information regarding the incorporated functional groups, Raman spectroscopy gives insights into the surface functionalization of SWCNT, MWCNT, and graphene.[20] Upon 785 nm excitation of pristine SWCNT, **SWCNT-1**, and **SWCNT-2** the three most important signatures of these hollow cylinders are noted. Firstly, the radial breathing modes bands (RBM) between 186 and 270

cm^{-1} suggest the presence of both metallic and semiconducting SWCNTs with a range of diameters between 0.8 and 1.4 nm. Secondly, the D mode is located between 1290 cm^{-1} and 1300 cm^{-1}. Finally, the G mode or MT-tangential mode is seen between 1592-1595 cm^{-1} (Figure S3). Upon covalent functionalization the D band increases due to the re-hybridization of carbon atoms from sp^2 to sp^3. Importantly, the I_D/I_G ratio (Table inserted in Figure S3) is used to quantify the amount of covalently anchored groups. The latter increases from 0.064 for pristine SWCNT to 0.283 for **SWCNT-1**. For **SWCNT-2**, the I_D/I_G ratio remains, however, constant with 0.284. As such, the subsequent click reaction takes only place with the alkyne groups previously anchored to SWCNT. Moreover, the G tangential mode experiences a small up-shift (1-2 nm) going from pristine SWCNT to **SWCNT-1** and **SWCNT-2**. This is in sound agreement with previous findings regarding the non-covalent modification of SWCNT with exTTF-based receptors.[13b,21]

In contrast to SWCNTs, the intensity ratio between the D and G bands for MWCNTs increases only slightly from MWCNT to **MWCNT-2**, although the broader G band includes contributions from disorder, defects, or intercalation between CNT walls (Figure S4).[22]

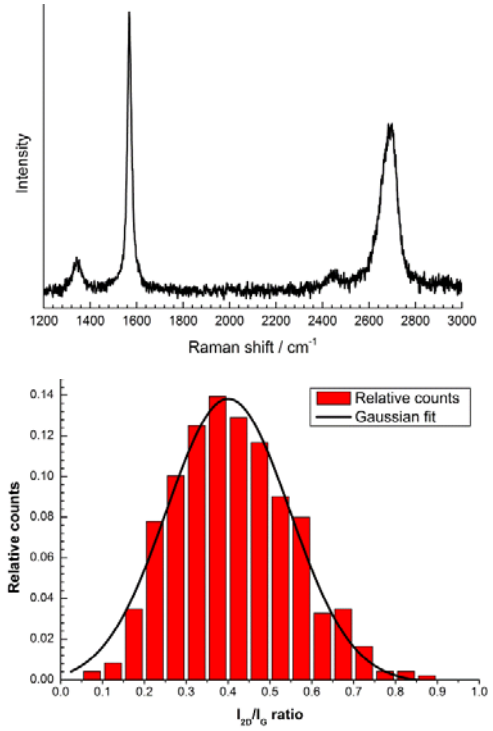

Figure 2. Raman spectrum of **GR-2** on top. Bottom, histogram with relative counts vs. I_{2D}/I_G ratio and the corresponding Gaussian distribution. The sample was drop casted from a DMF dispersion onto SiO_2 wafer and was excited at 532 nm.

Graphene samples excited at 532 nm reveal the typical Raman peaks of exfoliated graphite, namely, the D-, G-, and 2D-bands centered around 1340, 1565, and 2678 cm^{-1}, respectively. Upon exfoliation, a slight increase in the D band intensity is noticed due to defects induced by the ultrasonication process. A significant change in the shape and intensity of the 2D peak compared to bulk graphite is observed (Figure S5). The 2D band obtained with full width at half maximum (FWHM) values of 76 cm^{-1} was fit with 6 different Lorentzian functions with a FWHM of 24 cm^{-1}, which corresponds to graphene.[22] In addition, functionalization of the basal plane of graphene to form sp^3 domains contributes as well to an increase of the D band intensity (Figure S6). In analogy to SWCNT functionalization, graphenic materials present an I_D/I_G increase from 0.051 to 0.18 after Tour reaction in **GR-1**, but remain constant for **GR-2**. This result, with a much lower difference on the I_D/I_G ratio upon functionalization of graphene compared to SWCNT, highlights the lower reactivity of graphene under similar reaction conditions.[23] Figure 2 shows a typical Raman spectrum of **GR-2** and a statistical distribution of I_{2D}/I_G intensity ratio for a **GR-2** suspension drop casted onto SiO_2. The statistical distribution of I_{2D}/I_G is best fit with a Gaussian distribution function, which peaks at a ratio of 0.4. For bulk graphite or few-to multi-layer graphene the intensity ratio is 0.7 or less.[24] As such, the Raman spectra prompt to predominantly few-layer graphene, which likely originate from the initial exfoliation step performed with NMP. In sound agreement with the transmission electron microscopy (TEM) measurements – vide infra – we concluded that we are dealing, at least upon drop casting, mainly with few-to multi-layer graphene.

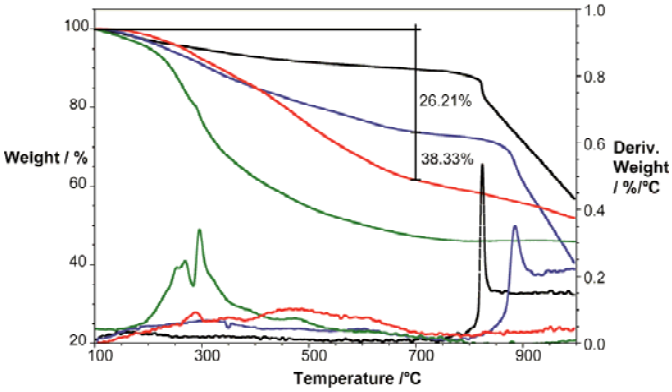

Figure 3. TGA and first derivative curves of pristine SWCNT (black), nanoconjugates **SWCNT-1** (blue) and **SWCNT-2** (red), together with the thermal decomposition of the exTTF molecule **2** (green) recorded under inert conditions.

To estimate the grafting density, thermogravimetric analysis (TGA) measurements were performed. A significantly higher degree of functionalization was obtained for **SWCNT-1** (Figure 3) when compared to **MWCNT-1** (Figure S7) and **GR-1** (Figure S8) under similar reaction conditions. More specifically, the weight loss measured for the thermal decomposition of the phenylacetylene groups in **SWCNT-1** was 26 % compared to 8 % for **MWCNT-1** and 14 % for **GR-1**. As expected, the carbon nanostructure reactivities were found to depend on their topography. A higher curvature in, for example, SWCNTs renders them more favorable for covalent chemical reactions than MWCNT or graphene sheets. Moreover, the linkage of the electron-donor exTTF via click reaction increases the observed weight loss. The total decomposition due to the **SWCNT-2** functionalization was 38 %, which refers to a 12 % increase compared to **SWCNT-1**. From this we estimate 1 functional group per 72 C atoms. For **MWCNT-2**, the weight loss is 21 % (29.6 % total weight loss), which corresponds to 1 functional group per 106 C atoms. For **GR-2**, the weight loss of 6.9 % (21.3 % total weight loss) corresponds to 1 functional group per 168 C

atoms (see Figure S9 for a direct comparison on the TGA curves of the three functionalized **CNF-2**).[25] In summary, TGA measurements provided first insights into the efficiency of the click reaction and suggested that not all phenylacetylene groups were further functionalized through the copper catalyzed click reaction.

X-ray photoelectron spectroscopy (XPS) further demonstrated the successful functionalization of the carbon nanoforms. The spectra of **SWCNT-2** (Figure S10), **MWCNT-2** (Figure 4), and **GR-2** (Figure S11) display the spectroscopic signatures of carbon, oxygen, nitrogen, sulfur, and silicon. Upon treatment with 4-(2-trimethylsilyl)ethynylaniline and isoamyl nitrite, a significant amount of Si 2p was detected in the XPS spectra for **SWCNT-1**, **MWCNT-1**, and **GR-1**, stemming from the alkyne protecting group after Tour reaction. An important observation is the lack of nitrogen in the intermediate samples, confirming the absence of unreacted species, which were removed during the work-up. In stark contrast, nitrogen is discernible in **SWCNT-2**, **MWCNT-2**, and **GR-2** samples. The deconvolution of the C1s energy level signals was accomplished with five Gaussian-Lorentzian curves, which were attributed to the various carbon atoms (C sp, C sp^2 and C sp^3, C=O, and C-O) present in the carbon nanoforms (Figure 4, inserted).[26] The deconvolution of the N 1s energy level signal, for **SWCNT-2**, **MWCNT-2**, and **GR-2** let to two peaks. For **MWCNT-2** (Figure 4), the first peak located at 401.5 eV is attributed to one nitrogen atom of the triazole ring, while the other two nitrogen atoms give rise to the second peak at 400.1 eV.[27] An analogous behavior was observed for **SWCNT-2** and **GR-2** (Figures S10 and S11). The absence of the peak corresponding to the free azide groups at 405.0 eV unambiguously proves that the azido exTTF is covalently attached to the carbon nanomaterials rather than beeing simply physisorbed onto the surface by π-stacking interactions.[28] A single S 2p signal at around 170 eV was found for the samples subjected to the click reaction, indicating the presence of sulfur from the organic electron-donor. In line with the results discussed for TGA – vide supra – the Si 2p peak is still observable for **SWCNT-2**, **MWCNT-2**, and **GR-2**. Nevertheless, its atomic percentage indicates an important decrease compared to the amount of Si observed in the intermediate products, suggesting a non-complete deprotection of the alkyne group and, therefore, a non-quantitative click reaction.

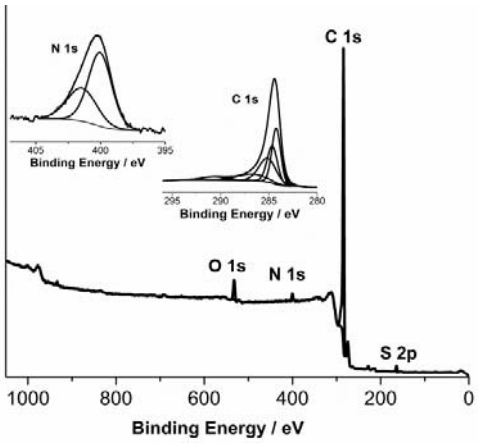

Figure 4. XPS spectrum of **MWCNT-2** and deconvoluted XPS core level spectra of carbon C 1s and N 1s.

To complement the characterization of the nanoconjugates, TEM investigations were employed to study their morphology. On one hand, detailed analyses of pristine SWCNT revealed mostly the presence of SWCNT bundles. **SWCNT-1** and **SWCNT-2**, on the other hand, appear with larger diameter, and smaller bundles that coexist with the presence of individual SWCNT, as a result of the effective functionalization (Figure S12). This finding is in line with the increase in intensity of the D-mode in the Raman spectra (Figure S3). On the other hand, the general aspects of the pristine and functionalized MWCNT are similar in terms of diameter and length (Figure S13).

Graphite exfoliation up to micrometer-sized graphene flakes with thickness of bi-or tri-layer graphene was supported by TEM microscopic analysis (Figure S14). However, reaggregation of graphene flakes prior to functionalization was only partially prevented by keeping the sample in solution, since **GR-2** samples reveal few-layer graphene sheets, which appear crumbled and intertwined (Figure 5).

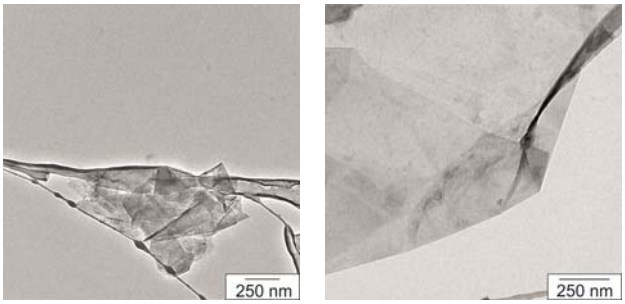

Figure 5. TEM images of **GR-2** drop casted from a DMF dispersion onto a lacey carbon grid.

The electrochemical properties of **SWCNT-2**, **MWCNT-2** and **GR-2** materials were studied by cyclic voltammetry (CV) and compared with a reference sample of exTTF **2**. In all samples, the single two-electron and chemically quasi-reversible oxidation of the exTTF unit to form dicationic species is clearly discernible.[11] The oxidations are noticeably broader and positively shifted by 220-270 mV relative to the reference system **2** (Figure 6), which is likely to be a result of the intramolecular electronic interaction between the electroactive units (CNF and exTTF) in the nanoconjugates, as previously observed in related samples.[13a,b, 29]

To further evaluate the impact of the covalent functionalization on the electronic properties of the carbon nanoforms synthesized and to investigate the possibility of the formation of radical ion pairs that include the oxidation of exTTF, and the reduction of the different carbon nanoforms, we employed absorption, emission, and transient absorption spectroscopy.

When different SWCNT, **SWCNT-1** and **SWCNT-2** suspension in *N*,*N*-dimethylformamide (DMF) were investigated by absorption spectroscopy, in line with previous studies,[30] the absorption features of covalently functionalized SWCNT are notably blue shifted when compared to the pristine sample (Figure 7). In particular, SWCNT reveals absorption maxima at 560, 661, 741, 814, 1006, 1072, 1172, and 1313 nm. After SWCNT functionalization, the transitions at higher energies in, for example, **SWCNT-1** undergo slight hypsochromic shifts to 558, 652, 733, and 812 nm, while those at lower energies are shifted appreciably stronger, that is, to 989, 1051, 1145, and 1279 nm. The absorption spectrum of **SWCNT-2** reveals only a minor

shift to 557, 655, 734, 810, 998, 1054, 1154, and 1287 nm. This is likely due to a redistribution of charge density within the covalently functionalized SWCNT.

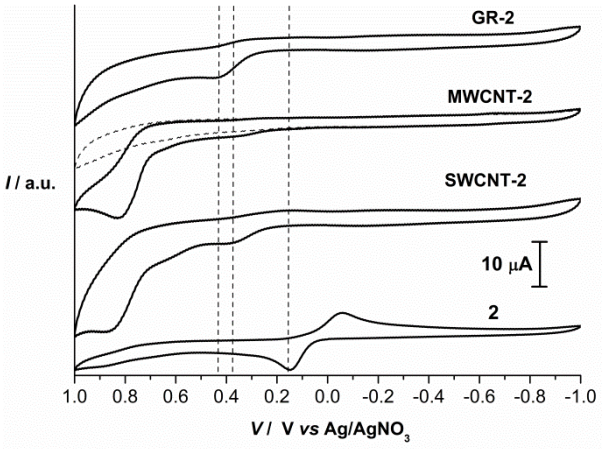

Figure 6. Cyclic voltammograms of **SWCNT-2**, **MWCNT-2**, **GR-2** and reference exTTF **2**, obtained in DMF solutions containing 0.1 M $TBAPF_6$ and using $Ag/AgNO_3$ as reference electrode, glassy carbon as working electrode and a Pt wire counter electrode. Scan rate is 100 mV/s. The dashed line corresponds to the background signal.

In addition to the absorption assays, we subjected pristine SWCNTs, **SWCNT-1** and **SWCNT-2** to fluorescence measurements in DMF. Accordingly, measurements performed with pristine SWCNTs reveal maxima at 1057, 1128, 1211, 1305, and 1419 nm, which correspond to (10,2), (7,6), (11,3), (13,2), and (9,8) SWCNT, respectively (Figure 8).[31] It is important to note that the fluorescence features mirror image those seen in the absorption measurements. For **SWCNT-1** and **SWCNT-2**, a similar fluorescence pattern was found with just minor hypsochromic shifts relative to pristine SWCNT (Figure 8). Moreover, the comparison between the fluorescence of the functionalized SWCNT with that of pristine SWCNT at equal absorbances at the excitation wavelength, as shown in Figure 9, unravels quenching of the SWCNT fluorescent features. As a matter of fact, the fluorescence intensities of **SWCNT-1** and **SWCNT-2** are quenched, with values of 82 and 63 %, respectively, relative to pristine SWCNT. While the fluorescence quenching between SWCNT and **SWCNT-1** is due to functionalization, the quenching, which relates to a comparison between SWCNT and **SWCNT-2,** has the additional contribution from an energy and/or electron transfer.

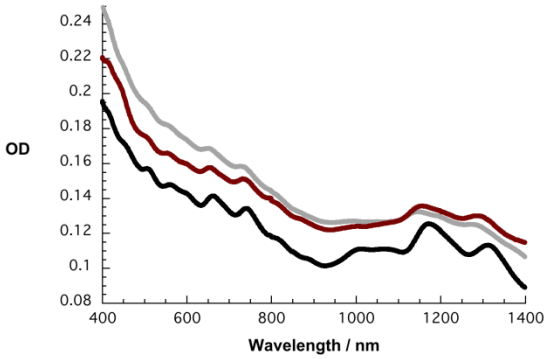

Figure 7. Absorption spectra of SWCNT (black), **SWCNT-1** (grey), and **SWCNT-2** (red) in DMF.

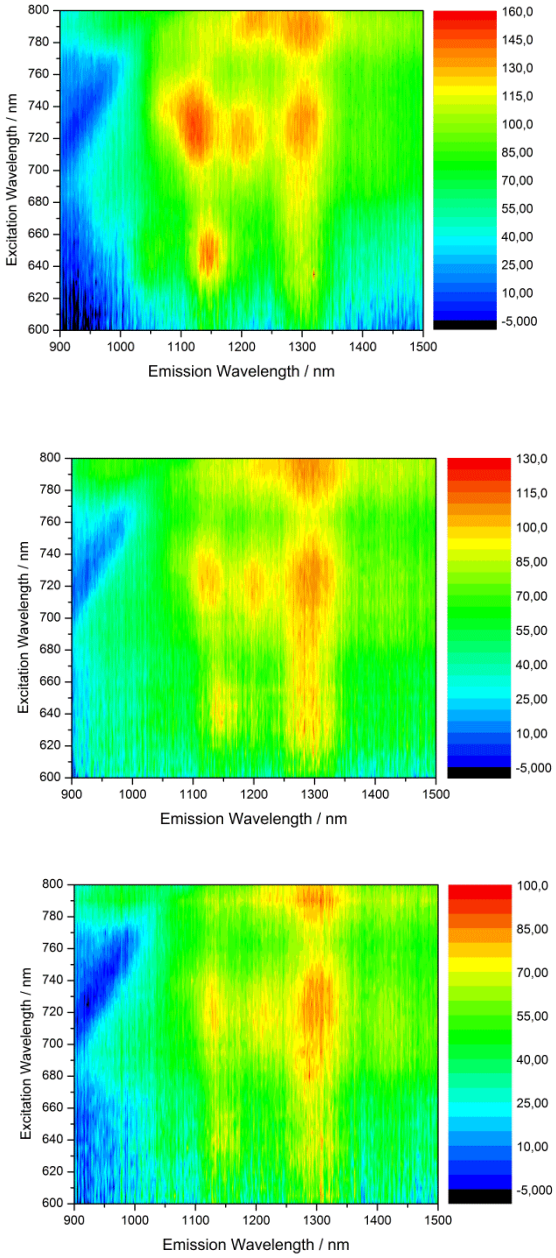

Figure 8. 3D steady-state fluorescence spectra of pristine SWCNT (top), **SWCNT-1** (middle), and **SWCNT-2** (bottom) in DMF with increasing intensity from blue to green to yellow and to red.

Strong support for excited state interactions, that is, between exTTF as electron donor and SWCNT as excited state electron acceptor came from femtosecond transient absorption measurements. Looking at SWCNT, which were simply suspended in DMF, a set of transient minima were observed at 455, 515, 565, 570, 665, 1195, 1315, and 1375 nm (Figure S15). In other words, a negative imprint of the van Hove singularities evolves. As Figure S15 shows, all features decay similarly during the recovery of the ground state with two major lifetime components (i.e., 1.5 and 80 ps). Overall, no particular shifts of the transitions were observable during the decay. Notably, this behavior resembles that seen numerously for pristine SWCNT suspended in various solvents. When turning to **SWCNT-1**, minima at 455, 510, 560, 570, 660, 1190, 1310, and 1360 nm

were noted upon 387 nm excitation (Figure S16). The features are hypsochromically shifted when compared to pristine SWCNT – a finding that reflects the influence noted in the ground state absorption. From a multiwavelength analysis we derive major lifetime components for the excited state decay with values of 1.5 and 65 ps. The overall difference in terms of lifetimes relative to pristine SWCNT relates to the impact that the functionalization exerts on the electron properties of SWCNT. Finally, for **SWCNT-2** we note the same minima at 455, 510, 560, 570, 660, 1185, 1310, and 1360 nm at the conclusion of the excitation (Figure 10). Unlike what it is seen for **SWCNT-1**, in which minima decay with 1.5 and 65 ps, in **SWCNT-2** a major decay takes place with a lifetime of 15 ps. Overall, appreciable blue shifts of the transient bleaching with minima at 500, 554, 650, 1175 and 1360 nm evolve in this deactivation. Implicit are new conduction bands, in which electrons are injected from exTTF shifting the transitions to lower energies. Important is also the 600 to 800 nm range, where a new transition correlates well with the one-electron oxidized exTTF.[32] In other words, the lifetime of 15 ps in **SWCNT-2** correlates with a charge separation. A global analysis resulted in a lifetime of this newly generated radical ion pair state of about 250 ps.

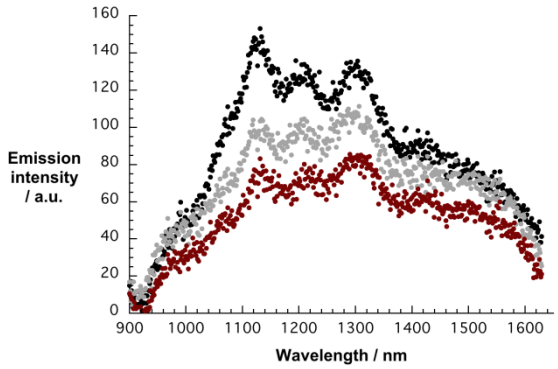

Figure 9. Comparison of the NIR fluorescence spectra of pristine SWCNT (black), **SWCNT-1** (grey) and **SWCNT-2** (red) in DMF – 720 nm excitation.

Unfortunately, the lower degree of functionalization achieved in MWCNT and graphene samples do not allowed a proper photophysical characterization of the aggregates formed. As a matter of fact, following photoexcitation at 387 nm, the differential absorption spectra of **GR-2** are like those seen for the starting material, that is, exfoliated graphite (Figure S17). In the visible, we note an ultrashort lived transient – in the form of bleaching – between 550 and 800 nm. This transient transforms within 0.5 ps to a featureless and broad transient. In the near-infrared, a distinct bleaching evolves between 800 and 1400 nm and beyond. It is formed with approximately 0.5 ps and can be assigned to a graphite-related phonon bleaching. A closer look at the kinetics at, for example, 625 and 1100 nm reveals that the transformation of the earlier is linked to the formation of the latter. Nevertheless, both decay monoexponentially to reinstate the baseline. From the lack of any metastable transient, on one hand, and that neither spectroscopic nor kinetic differences emerge relative to exfoliated graphite, on the other hand, we conclude the absence of electron transfer in photoexcited **GR-2**.

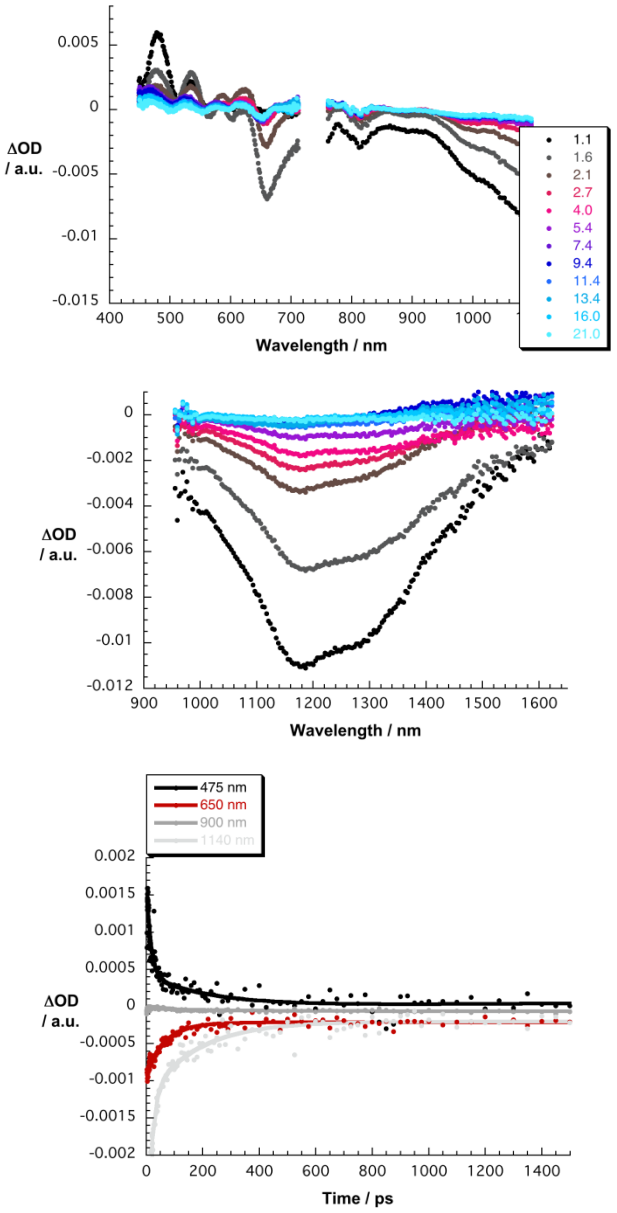

Figure 10. Upper part – differential absorption spectra (visible and near-infrared) obtained upon femtosecond pump probe experiments (387 nm) of **SWCNT-2** with several time delays between 1.1 and 21.0 ps at room temperature. Central part – differential absorption spectra (extended near-infrared) obtained upon femtosecond pump probe experiments (387 nm) of **SWCNT-2** with several time delays between 1.1 and 21.0 ps at room temperature. Lower part – time absorption profiles of the spectra shown in the upper part at 475, 650, 900, and 1140 nm monitoring the charge separation and charge recombination.

Conclusions

We presented here a comprehensive assay on the covalent functionalization of carbon nanoforms by means of the well-established CuAAC reaction. To this end, phenylethinyl-decorated SWCNTs, MWCNTs, and graphene were prepared by arylation with diazonium salts under mild conditions in very good yields. All intermediates and materials were characterized by FTIR, Raman spectroscopy, TGA, and XPS analysis as well as by

TEM microscopy.

Furthermore, by this covalent method, we have functionalized SWCNTs, MWCNTs and graphene with an electroactive molecule, namely i.e. exTTF, which is evidently observed in the solution electrochemistry performed with all the materials. For **SWCNT-2**, where the density of exTTFs on the surface was the highest (1 per 72 C atoms), a new transition absorption maximum around 600 to 800 nm range is observed upon photoexcitation. Owing to the fact that the latter is an unambiguous attribute of the one-electron oxidized exTTF it documents the successful formation of the charge separated state.

Acknowledgements

Financial support from the European Research Council ERC-2012-ADG_20120216 (Chirallcarbon), MINECO of Spain (grant numbers CTQ2011-24652 and PIB2010JP-00196), MOLESCO (grant number 606728), and CAM (grant number MADRISOLAR-2 S2009/PPQ-1533) is greatly appreciated. N. M. is indebted to Alexander von Humboldt Foundation. We wish to thank Prof. Philippe Serp for providing us with MWCNT synthesized by the CVD method developed in his laboratory. M. M. O. acknowledges financial support from the Marie Curie COFUND programme "U-Mobility" co-financed by Universidad de Malaga and the European Community´s Seventh Framework Programme under Grant Agreement No. 246550.

Notes and references

[a] *Departamento de Química Orgánica I, Facultad de Química, Universidad Complutense, E-28040 Madrid, Spain. E-mail: maherran@quim.ucm.es, nazmar@quim.ucm.es*

[b] *Friedrich-Alexander-Universität Erlangen-Nürnberg, Department of Chemistry and Pharmacy & Interdisciplinary Center for Molecular Materials (ICMM), Egerlandstrasse 3, 91058 Erlangen, Germany. E-mail: guldi@chemie.uni-erlangen.de*

[c] *Current address: Organisch-Chemisches Institut, University of Heidelberg, Im Neuenheimer Feld 270, 69120 Heidelberg, Germany.*

[d] *IMDEA-Nanociencia, c/Faraday 9, Campus Cantoblanco, 28049 Madrid, Spain.*

† Electronic Supplementary Information (ESI) available: Experimental section, synthetic procedures, characterization data and selected supplementary figures.See DOI: 10.1039/b000000x/

‡ Dedicated to Professor Fernando Langa in celebration of his 60th birthday.

§ J. M.-G., L. R.-P. and M. M.-O. equally contributed to this article.

1. a) M. Sharon, M. Sharon, *Carbon Nano Forms and Applications*, McGraw-Hill, New York, 2010; b) D. M. Guldi, N. Martín, *Carbon Nanotubes and Related Structures*, Wiley-VCH, Weinheim, 2010; c) T. Akasaka, F. Wudl, S. Nagase, *Chemistry of Nanocarbons*, John Wiley&Sons, Chichester, 2010.
2. Special issues devoted to Graphene Chemistry, Properties and Application on *Acc. Chem. Res.*, 2013, **46**, 1 (pp. 1-189) and 10 (pp. 2191-2339).
3. H. W. Kroto, J. R. Heath, S. C. O'Brien, R. F. Curl, R. E. Smalley, E. *Nature* 1985, **318**, 162.
4. a) S. Iijima, *Nature*, 1991, **354**, 56; b) S. Iijima, T. Ichihashi, *Nature*, 1993, **363**, 603; c) D. S. Bethune, C. H. Klang, M. S. de Vries, G. Gorman, R. Savoy, J. Vasquez, R. Beyers, *Nature*, 1993, **363**, 605.
5. For reviews, see: a) D. Tasis, N. Tagmatarchis, A. Bianco, M. Prato, *Chem. Rev.,* 2006, **106**, 1105; b) Y.-L. Zhao, J. F. Stoddart, *Acc. Chem. Res.,* 2009, **42**, 1161; c) P. Singh, S. Campidelli, S. Giordani, D. Bonifazi, A. Bianco, M. Prato, *Chem. Soc. Rev.,* 2009, **38**, 2214; d) S. A. Hodge, M. K. Bayazit, K. S. Coleman, M. S. P. Shaffer, *Chem. Soc. Rev.,* 2012, **41**, 4409; e) L. Rodríguez-Pérez, M. A. Herranz, N. Martín, *Chem. Commun.,* 2013, **49**, 3721; f) K. Dirian, M. A. Herranz, G. Katsukis, J. Malig, L. Rodríguez-Pérez, C. Romero-Nieto, V. Strauss, N. Martín, D. M. Guldi, *Chem. Sci.,* 2013, **4**, 4335; g) E. Vázquez, F. Giacalone, M. Prato, *Chem. Soc. Rev.*, 2014, **43**, 58.
6. N. Komatsu, F. Wang, *Materials,* 2010, **3**, 3818.
7. F. Wang, T. M. Swager, *J. Am. Chem. Soc.,* 2011, **133**, 11181.
8. A. Hirsch, O. Vostrowsky *Top. Curr. Chem.* 2005, **245**, 193.
9. a) M.-Q. Yang, N. Zhang, Y.-J. Xu, *ACS Appl. Mater. Interfaces*, 2013, **5**, 1156; b) N. Zhang, Y. Zhang, M.-Q. Yang, Z.-R. Tang, Y.-J. Xu, *Journal of Catalysis*, 2013, **299**, 210; c) M.-E. Ragoussi, S. Casado, R. Ribeiro-Viana, G. de la Torre, J. Rojo, T. Torres, *Chem. Sci.,* 2013, **4**, 4035; d) M.-E. Ragoussi, G. Katsukis, A. Roth, J. Malig, G. de la Torre, D. M. Guldi, T. Torres, *J. Am. Chem. Soc.,* 2014, **136**, 4593.
10. a) G. Clavè, S. Campidelli, *Chem. Sci.,* 2011, **2**, 1887; b) H.-X. Wang, K.-G. Zhou, Y.-L. Xie, J. Zeng, N.-N. Chai, J. Li, H.-L. Zhang, *Chem. Commun.,* 2011, **47**, 5747; c) G. Tuci, C. Vinattieri, L. Luconi, M. Ceppatelli, S. Cicchi, A. Brandi, J. Filippi, M. Melucci, G. Giambastiani, *Chem. Eur. J.,* 2012, **18**, 8454; d) I. Hijazi, B. Jousselme, P. Jégou, A. Filoramo, S. Campidelli, *J. Mater. Chem.,* 2012, **22**, 20936; e) M. Castelaín, G. Martínez, C. Marco, G. Ellis, H. J. Salavagione, *Macromolecules*, 2013, **46**, 8980; f) S. G. Yenchalwar; R. R. Devarapalli, A. B. Deshmukh, M. V. Shelke, *Chem. Eur. J.,* 2014, **20**, 7402.
11. F. G. Brunetti, J. L. López, C. Atienza, N. Martín, *J. Mater. Chem.,* 2012, **22**, 4188.
12. For examples with fullerenes: a) N. Martín, L. Sánchez, M. A. Herranz, B. M. Illescas, D. M. Guldi, *Acc. Chem. Res.,* 2007, **40**, 1015; b) S. Castellanos, A. A. Vieira, B. M. Illescas, V. Sacchetti, C. Schubert, J. Moreno, D. M. Guldi, S. Hecht, N. Martín, *Angew. Chem. Int. Ed*., 2013, **52**, 13985; c) M. Wielopolski, A. Molina-Ontoria, C. Schubert, J. T. Margraf, E. Krokos, J. Kirschner, A. Gouloumis, T. Clark, D. M. Guldi, N. Martín, *J. Am. Chem. Soc.,* 2013, **135**, 10372.
13. For examples with CNT: a) M. A. Herranz, N. Martín, S. Campidelli, M. Prato, G. Brehm, D. M. Guldi, *Angew. Chem. Int. Ed.,* 2006, **45**, 4478; b) M. A. Herranz, C. Ehli, S. Campidelli, M. Gutiérrez, G. L. Hug, K. Ohkubo, S. Fukuzumi, M. Prato, N. Martín, D. M. Guldi, *J. Am. Chem. Soc.,* 2008, **130**, 66; c) C. Romero-Nieto, R. García, M. A. Herranz, C. Ehli, M. Ruppert, A. Hirsch, D. M. Guldi, N. Martín, *J. Am. Chem. Soc.*, 2012, **134**, 9183; d) F. G. Brunetti, C. Romero-Nieto, J. López-Andarias, C. Atienza, J. L. López, D. M. Guldi, N. Martín, *Angew. Chem. Int. Ed.*, 2013, **52**, 2180; e) J. López-Andarias, J. L. López, C. Atienza, F. G. Brunetti, C. Romero-Nieto, D. M. Guldi, N. Martín, N. *Nat. Commun.*, 2014, **5**, 3763.
14. S. González, N. Martín, A. Swartz, D. M. Guldi, *Org. Lett.,* 2003, **5**, 557.
15. J. L. Bahr, J. Yang, D. V. Kosynkin, M. J. Bronikowski, R. E. Smalley, J. M. Tour, *J. Am. Chem. Soc*., 2001, **123**, 6536.
16. B. K. Price, J. M. Tour, *J. Am. Chem. Soc.,* 2006, **128**, 12899.
17. Y. Hernandez, V. Nicolosi, M. Lotya, F. M. Blighe, Z. Sun, S. De, I. T. McGovern, B. Holland, M. Byrne, Y. K. Gun'Ko, J. J. Boland, P. Niraj, G. Duesberg, S. Krishnamurthy, R. Goodhue, J. Hutchison, V. Scardaci, A. C. Ferrari, J. N. Coleman, *Nat. Nanotechnol*., 2008, **3**, 563.
18. E. Pretsch, P. Buhlmann, M. Badertscher, *Structure Determination of Organic Compounds*, Springer, Berlin and Heidelberg, 2009.
19. The shifts and broadness observed in the skeletal in-plane vibrations of the different carbon nanoforms are due to different contributions: changes of the interplane bonding, disorder and finite size effects, or bending of the graphitic sheets. See for example: J. Kastner, T. Pichler, H. Kuzmany, S. Curran, W. Blau, D. N. Weldon, M. Delamesiere, S. Draper, H. Zandbergen, *Chem. Phys. Lett.,* 1994, **221**, 53.
20. a) R. Graupner, *J. Raman Spectrosc.*, 2007, **38**, 673; b) M. S. Dresselhaus, G. Dresselhaus, A. Jorio, A. G. Souza Filho, M. A. Pimenta, R. Saito, *Acc. Chem. Res*., 2002, **35**, 1070.
21. A. de Juan, Y. Pouillon, L. Ruiz-González, A. Torres-Pardo, S. Casado, N. Martín, A. Rubio, E. M. Pérez, *Angew. Chem. Int. Ed.,* 2014, **53**, 5394.

22. L. M. Malard, M. A. Pimenta, G. Dresselhaus, M. S. Dresselhaus, *Phys. Rep.*, 2009, **473**, 51.
23. M. S. Dresselhaus, A. Jorio, M. Hofmann, G. Dresselhaus, R. Saito, *Nano Lett.*, 2010, **10**, 751.
24. A. C. Ferrari, J. C. Meyer, V. Scardaci, C. Casiraghi, M. Lazzeri, F. Mauri, S. Piscanec, D. Jiang, K. S. Novoselov, S. Roth, A. K. Geim, *Phys. Rev. Lett*., 2006, **97**, 187401.
25. In the case of MWCNT and graphene samples, the estimation of real surface functionalization is less accurate considering the fact that the inner layers remain unfunctionalized.
26. M. E. Lipinska, S. L. H. Rebelo, M F. R. Pereira, J. A. N. F. Gomes, C. Freire, J. L. Figueiredo, *Carbon*, 2012, **50**, 3280.
27. S. Ciampi, T. Böcking, K. A. Kilian, M. James, J. B. Harper, J. J. Gooding, *Langmuir*, 2007, **23**, 9320.
28. J. P. Collman, N. K. Devaraj, T. P. A. Eberspacher, C. E. Chidsey, E. D. *Langmuir*, 2006, **22**, 2457.
29. S. P. Economopoulos, G. Rotas, Y. Miyata, H. Shinohara, N. Tagmatarchis, *ACS Nano*, 2010, **4**, 7499.
30. B. Gebhardt, Z. Syrgiannis, C. Backes, R. Graupner, F. Hauke, A. Hirsch, *J. Am. Chem. Soc*., 2011, **133**, 7985.
31. S. M. Bachilo, M. S. Strano, C. Kittrell, R. H. Hauge, R. E. Smalley, R. B. Weisman, *Science*, 2002, **298**, 2361.
32. D. M. Guldi, L. Sánchez, N. Martín, *J. Phys. Chem. B*, 2001, **105**, 7139.

Cite this: DOI: 10.1039/c0xx00000x

www.rsc.org/xxxxxx

PAPER

Table of contents entry

The different reactivity of carbon nanoforms such as SWCNT, MWCNT and graphene involving sequential arylation and click chemistry reactions has important consequences on the properties of the nanoconjugates obtained with electroactive units.